A new look on the “Valid Detection Probability” of PIV Vectors

Scharnowski, Sven; Sciacchitano, Andrea; Kähler, Christian J.

Publication date
2018

Document Version
Final published version

Published in
Proceedings of the 19th international symposium on application of laser and imaging techniques to fluid mechanics

Citation (APA)
Scharnowski, S., Sciacchitano, A., & Kähler, C. J. (2018). A new look on the “Valid Detection Probability” of PIV Vectors. In *Proceedings of the 19th international symposium on application of laser and imaging techniques to fluid mechanics*

A new look on the "Valid Detection Probability" of PIV Vectors

Sven Scharnowski[1*], Andrea Sciacchitano[2] , Christian J. Kähler[1]
1: Institute of Fluid Mechanics and Aerodynamics, Bundeswehr University Munich, 85577 Neubiberg, Germany
2: Delft University of Technology, 2629HS Delft, The Netherlands
* Correspondent author: sven.scharnowski@unibw.de

Keywords: PIV, cross-correlation function, effective number of particle images

ABSTRACT

For the reliable estimation of velocity vector fields by means of 2D and 3D particle image velocimetry (PIV), the cross-correlation functions calculated from the signal within each interrogation window must feature a distinct peak that represents the average shift of the particle image ensemble. A high valid detection probability (VDP) of the correct correlation peak is necessary in order to compute valid and accurate velocity fields. The following analysis shows the sensitivity of *VDP* on flow parameters as well as on evaluation parameters. The most important result is that the so-called effective number of particle images $N_I F_I F_O$ is not suited to predict the *VDP* in the case of moderate or strong out-of-plane motion. This can be explained by the fact that the *VDP* depends not only on the number of particle images correctly paired, but also on the number of particle images remaining without partner, which yield spurious correlation peaks. The findings help to better understand the occurrence of false vectors and enable the PIV user to improve the measurement setup as well as the PIV evaluation in order to minimize spurious vectors.

1. Introduction

In particle image velocimetry (PIV) the velocity of a group of particles is estimated from the cross-correlation function of two interrogation windows containing the corresponding particle images at two consecutive time instants. Under ideal conditions, the sub-pixel location of the highest correlation value corresponds to the displacement of the particle image ensemble within the interrogation window. However, this only holds for the case where the flow within the interrogation window is uniform as well as homogenously seeded and a sufficient large number of particle images from two corresponding images can be paired. Keane and Adrian (1992) showed that the formation of a well detectable correlation peak is very likely if the number of particle images within the interrogation window is $N_I \geq 5$. For $N_I < 5$, the likelyhood that a random peak in the correlation function, that does not correspond to the correct particle image displacement, is higher than the one corresponding to the displacement, increases strongly.

For realistic PIV images, the loss-of-correlation due to in-plane motion F_I, out-of-plane motion F_O, displacement gradients F_Δ or image noise F_σ lead to a decreased probability for the detection of valid displacement vectors (Adrian and Westerweel, 2010, Raffel et al, 2018, Westerweel, 2008, Scharnowski and Kähler, 2016a/ 2016b). Keane and Adrian concluded that the loss of correlation can be compensated by increasing the number of particle images N_I such that:

$$N_\mathrm{I} F_\mathrm{I} F_\mathrm{O} \geq 5 \tag{1}$$

The product $N_\mathrm{I} F_\mathrm{I} F_\mathrm{O}$ is the so-called effective number of particle images according to Keane and Adrian (1992).

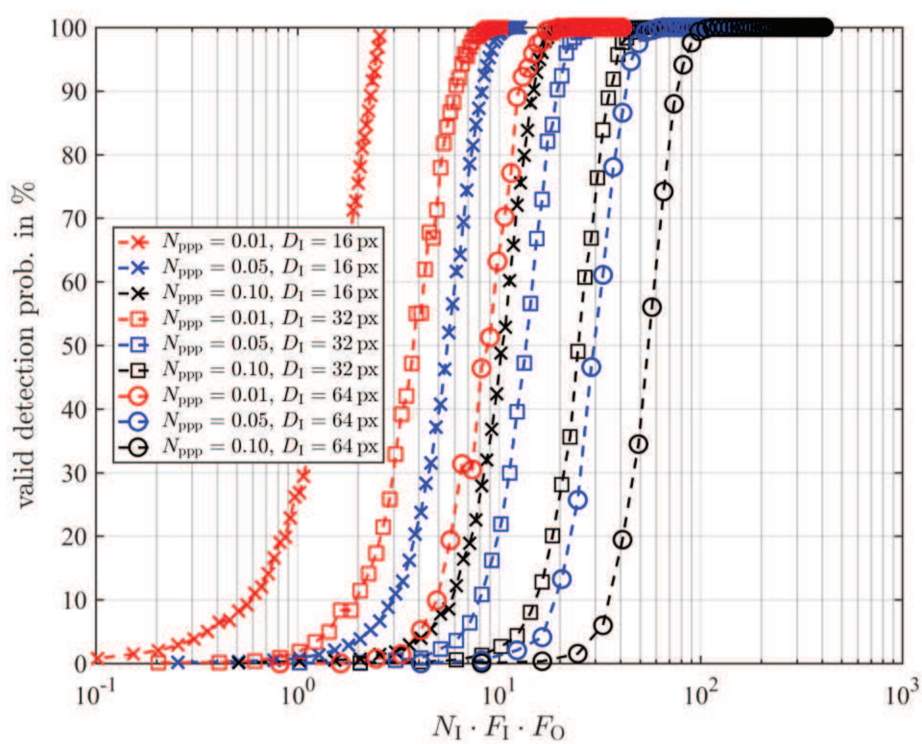

Fig. 1 Valid vector detection probability as a function of the effective number of particle images $N_\mathrm{I} F_\mathrm{I} F_\mathrm{O}$ for synthetic PIV images with zero in-plane motion ($F_\mathrm{I} = 1$) and varying out-of-plane motion for different particle image densities N_ppp and interrogation window sizes D_I.

New investigations show that relation (1) is not sufficient if the number of unpaired particle images is of the same order as the number of paired ones or even higher. This is however relevant for many realistic experiments where the time between the two illuminations is optimized for low uncertainty and high spatial resolution. To achieve a low uncertainty and high spatial resolution at the same time, the particle image displacement must be large compared to the random error of the evaluation method. Additionally, the light sheet must be thin and the interrogation windows must be small to achieve good out-of-plane and in-plane resolution, respectively. However, a large displacement in a thin light sheet also increases the probability of loss-of-pairs due to in-plane and out-of-plane motion and thus decreases F_I and F_O. Figure 1 illustrates how the valid detection probability changes with respect to the effective number of particle images over a wide range of particle image densities and interrogation window sizes. The valid detection probability is the probability with that the highest correaltion peak corresponds to the true mean displacement of the particle image ensemble. It was evaluated from O(1000) correlation functions computed from synthetic PIV images for each data point in the figure.

It can be concluded from Fig. 1 that the product $N_\mathrm{I}F_\mathrm{I}F_\mathrm{O}$ is not useful in general to determine the effective number of particle images. Especially if N_I is relatively large and F_O is relatively small the unpaired particle images affect the correlation function significantly. For example $N_\mathrm{I}=10$ and $F_\mathrm{O}=1$ (red squares in Fig. 1) does not result in the same valid detection probability as $N_\mathrm{I}=100$ and $F_\mathrm{O}=0.1$ (black squares in Fig. 1). Although the product $N_\mathrm{I}F_\mathrm{I}F_\mathrm{O}$ is constant, the valid detection probability decreases from 100% to about 3%. Thus, the rule of thumb that predicts a valid detection probability of $>95\%$ for $N_\mathrm{I}F_\mathrm{I}F_\mathrm{O}\geq 5$, does not apply for a broad range of parameters.

In order to understand why the so-called effective number of particle images is not sufficient to predict the valid detection probability, correlation functions of synthetic PIV images were analyzed systematically. The following section discusses the height distribution of the displacement peak as well as the secondary correlation peak and their relation to the valid detection probability. In Sec. 3 the effect of several image parameters on the valid detection probability is discussed in detail. Section 4 analyzes the possibility to optimize the interrogation window size depending on the flow and image parameters and conclusions are drawn in Sec. 5.

2. Correlation Peak Height Distribution & Valid Detection Probability

Figure 2 shows an example of a synthetic PIV image pair with a relative out-of-plane shift of $\Delta z/\Delta z_0=0.3$ corresponding to $F_\mathrm{O}=0.7$. The in-plane-shift was set to zero, simulating the final pass of a multi-pass evaluation. On average 12.8 particle images are found in each interrogation window size of $D_\mathrm{I}=16$ pixel for a particle image density of $N_\mathrm{ppp}=0.05$. However, as can be seen from the figure, the true number of particle images within each window varies significantly. For randomly chosen locations, the probability of finding exactly N_I particle image centers within a D_I^2 window is given by the binominal distribution:

$$pdf(N_\mathrm{I}, D_\mathrm{I}, N_\mathrm{ppp}) = \binom{N_\mathrm{I}}{D_\mathrm{I}^2} \cdot N_\mathrm{ppp}^{\;N_\mathrm{I}} \cdot \left(1 - N_\mathrm{ppp}\right)^{D_\mathrm{I}^2 - N_\mathrm{I}}, \tag{2}$$

where D_I is expressed in pixel. The distribution in Fig. 3 clearly shows a strong variation of N_I in agreement with the randomly distributed particle images in Fig. 2. The probability of finding 12 particle images within a window is about 11.4% but extrema values such as 6 and 20 particle images have still a significant probability of about 1.5%.

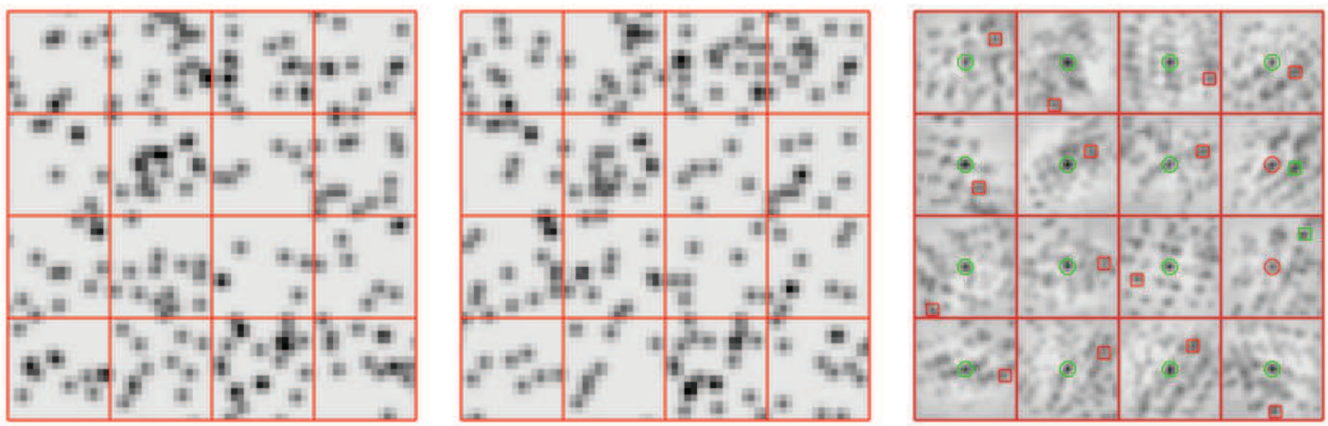

Fig. 2 Example PIV double image with a particle image diameter of $D = 3$ pixel, a particle image density of $N_\mathrm{ppp} = 0.05$ and an out-of-plane motion of $\Delta z / \Delta z_0 = 0.3$ (left and middle). Right: corresponding normalized correlation functions computed from an interrogation window size of $D_\mathrm{I} = 16$ pixel. The true displacement peak and the secondary peak are marked by circles and squares, respectively. Green and red color of the circles and squares indicates the highest and second highest peak, respectively.

Fig. 3 Probability density distribution of the number of particle images within a 16×16 pixel window for an average density of $N_\mathrm{ppp} = 0.05$.

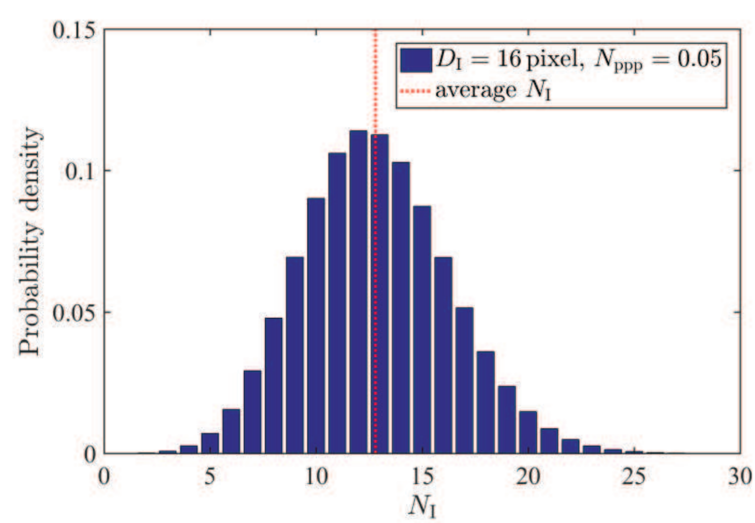

On the right side of Fig. 2 the normalized cross-correlation function of the two PIV images is shown qualitatively. The true displacement peak and the secondary peak are marked by circles and squares, respectively. Green color of the circle and squares indicates the highest peak while the second highest peak is colored in red. It can be seen from the figure that the secondary peak is sometimes higher than the displacement peak (refer to second and third row from top in the most right column). This is mainly caused by the loss-of-correlation due to out-of-plane motion. In the case of valid measurements, the displacement peak is higher than the secondary peak, and a valid vector is detected. Instead, when the secondary peak is larger than the displacement peak, an erroneous displacement vector (outlier or spurious vector) is computed.

Figure 4 illustrates the distribution of the height of the displacement peak and the secondary correlation peak for the case with significant out-of-plane shift $\Delta z / \Delta z_0 = 0.3$. The correlation peak heights were analyzed by means of synthetic PIV images with zero in-plane motion as shown in Fig. 2. The particle image diameter, the particle image density and the interrogation window size were set to $D = 3$ pixel, $N_{ppp} = 0.05$ and $D_I = 16$ pixel, respectively. Figure 4 shows that for the majority of correlation functions the displacement peak is higher than the secondary peak. However, for some cases the displacement peak becomes smaller than the secondary one, leading to an erroneous displacement vector. This is in agreement with the correlation functions presented in Fig. 2.

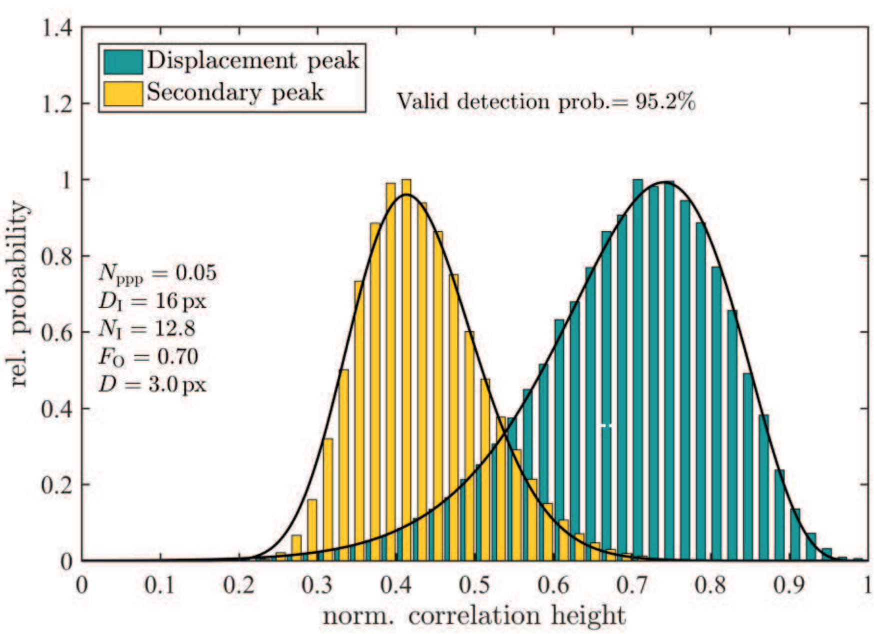

Fig. 4 Probability density distribution of the normalized correlation height for the displacement peak and the secondary peak for $D = 3$ pixel, $D_I = 16$ pixel, $N_{ppp} = 0.05$ and $F_O = 0.7$.

The actual value of the valid detection probability VDP depends on the probability density function of the displacement peak pdf_1 and of the secondary peak pdf_2 as follows:

$$VDP = \int_{-\infty}^{\infty} pdf_2(c_2) \cdot \int_{c_2}^{\infty} pdf_1(c_1)\, \mathrm{d}c_1\, \mathrm{d}c_2 \tag{3}$$

Where c_1 is the normalized height of the displacement peak and c_2 the normalized height of the secondary peak. For the case shown in Fig. 2 a valid detection probability of 95.2% is computed from the height distributions. Thus, for 4.8% of the cases the secondary peak becomes larger than the displacement peak.

3. Effect of Image and Flow Parameters on Correlation Statistic

Figure 5 shows the distributions of the displacement peak and the secondary correlation peak for a variation of the in-plane-motion (top left), the out-of-plane motion (middle left), the in-plane gradients (bottom left), the particle image density (top right), the interrogation window size (middle right) and the image noise level (bottom right).

Generally, it can be concluded from the figure that all parameters tested affect the valid detection probability of PIV vectors. It is important to note that the three parameters on the left hand side, F_I, F_O, and F_Δ, do not alter the probability of the secondary peak. This is due to the fact that the locations of the unpaired particle images are random. However, the width of the height distribution of the displacement peak increases with decreasing F_I, F_O, and F_Δ, indicating that a broader range of displacement peak heights becomes possible. If the displacement peak is always higher than the secondary peak the valid detection probability is unity. This is only the case if the distributions of both peak heights are well separated, as shown for $F_\mathrm{I} > 0.75$, $F_\mathrm{O} > 0.8$, $F_\Delta > 0.45$.

On the other hand, the parameters on the right side of Fig. 5, N_ppp, D_I, and SNR, clearly influence the distribution of both peaks. Figure 5 shows in the top right corner the effect of different particle image densities N_ppp on the correlation height distribution. The interrogation window size D_I was adjusted to keep the number of particle images N_I constant. The displacement correlation peak is not affected for $N_\mathrm{ppp} < 0.1$ because it is still composed of the same number particle images. For $N_\mathrm{ppp} > 0.1$ the particle images start to overlap massively leading to a slightly increasing width of pdf_1. The secondary peak however, strongly depends on N_ppp over the full range: the width and the mean value of the distribution increase with increasing particle image density.

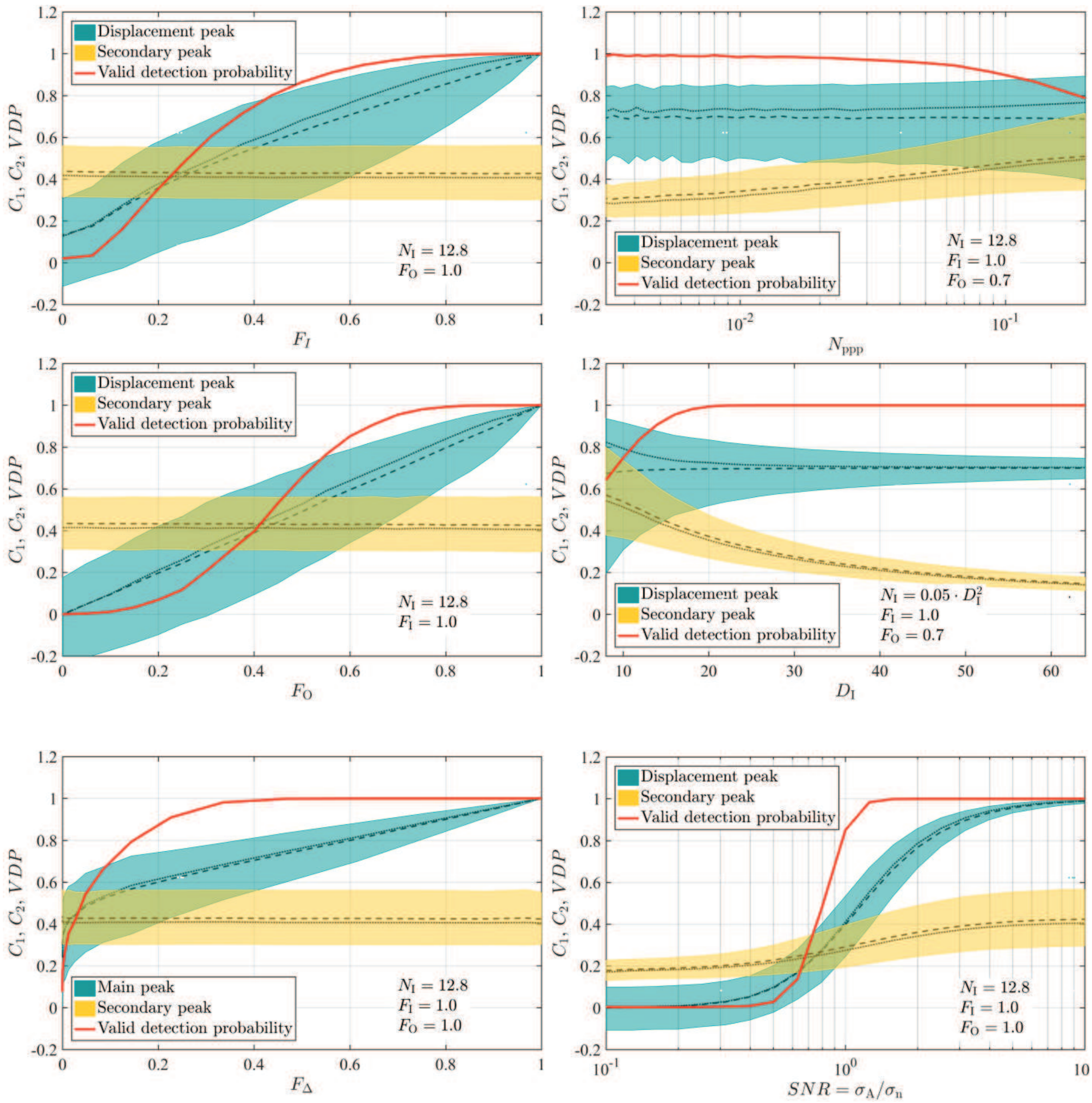

Fig. 5 Effect of F_I (top left), particle image density N_{ppp} (top right), F_O (middle left), interrogation window size D_I (middle right), F_Δ (bottom left) and signal-to-noise ratio SNR (bottom right) on the height distribution of the displacement peak and the secondary peak of the normalized cross-correlation function. If not varied, the simulation parameters are: $D_I = 16$ pixel, $N_{ppp} = 0.05$, $F_O = 0.7$, $SNR = 10$. The dotted lines and the dashed lines indicate the highest probability and the mean height, respectively. The shaded areas represent the 90% coverage of the *pdf* and the red solid line is the valid detection probability *VDP* from Eq. (3).

Besides the particle image density also the number of particle images within the interrogation window N_I influences the distribution of the secondary peak pdf_2. This is illustrated in Fig. 5 in the middle row on the right side for the evaluation of the same synthetic images with different interrogation window size ranging from $D_\mathrm{I} = 8$ pixel to 64 pixel. Additionally, N_I also affects the distribution of the displacement peak pdf_1: While its mean height is rather constant, the width and the height with the highest probability (dotted line) increase with decreasing window size. As a result, the valid detection probability decreases for smaller interrogation window sizes, as expected. The best spatial resolution is reached as soon as both pdf are separated, which is around $D_\mathrm{I} \approx 20$ pixel for the specific cases tested here.

Image noise reduces the normalized correlation height of the displacement peak and the secondary peak, as shown in Fig. 5 in the bottom right corner. In the relevant region $\sigma_\mathrm{A} / \sigma_\mathrm{n} > 1$ the height of the displacement peak decreases much faster than the secondary one. Here σ_A is the intensity standard deviation of the noise-free image and σ_n is the image noise level (see Scharnowski 2016b).

In summary it can be stated that the pdf of the displacement peak and the secondary correlation peak is quite sensitive on flow parameters, image parameters and evaluation parameters. As a result, the estimation of the valid detection probability becomes rather complex.

4. Optimized Interrogation Window Size

The strongest advantage of PIV over classical point-wise measurement techniques is its ability to provide flow fields from which the organization of turbulent structures of various length scales can be detected. In order to maximize the flow information acquired with PIV measurements, it is important to capture a large field of view and to resolve small details at the same time (Adrian, 1997; Kähler et al., 2012). To achieve this, camera sensors with a large number of pixel or multiple camera approaches (Cuvier 2017) can be combined with sophisticated image evaluation techniques that iteratively decrease the interrogation window size (Scarano, 2001; Sciacchitano et al. 2012).

The optimum interrogation window size depends on several factors: For the first evaluation step, the in-plane-motion as well as the in-plane gradients strongly affect the VDP. To account for this the shift of the particle image ensemble should not exceed one quarter of the interrogation window size for the first iteration (Keane and Adrian, 1990). For the following iterations the in-plane motion is compensated by window shifting and image deformation techniques so that the interrogation windows can be reduced in size from iteration to iteration.

The smallest suited window size for a reliable detection of the mean shift of the particle image ensemble within the interrogation window is reached if only $N_{\mathrm{I}} \approx 5$ particle images are found in each window on average (Keane and Adrian, 1992). Thus, the constraint of the particle image density limits the spatial resolution of PIV. If an out-of-plane motion is present the number of particle images within an interrogation window must be larger than 5 as illustrated in Fig. 1 to keep the valid detection probability on the same level. Additionally, for strong out-of-plane motions it is not sufficient to keep the product $N_{\mathrm{I}} F_{\mathrm{O}} > 5$, because the *VDP* also depends on the secondary correlation peak, which is formed from all particle images (see Fig. 4 and Eq. 3). Furthermore, as shown in Fig. 5 in the top right corner, the particle image density N_{ppp} influences the secondary correlation peak and thus the *VDP*.

The two parameters F_{O} and N_{ppp} are the driving parameters for determing the *VDP*. Figure 6 shows an example of the valid detection probability *VDP* as a function of F_{O} and N_{ppp} for an interrogation window of 16×16 pixel. It is clear from the figure, that a high valid detection probability (e.g. 95%) requires an increasing particle image density for smaller values of F_{O} in order to keep the spatial resolution constant. In other words: Depending on the out-of-plane motion and the particle image density, the interrogation window size must be selected to ensure a sufficiently high *VDP*.

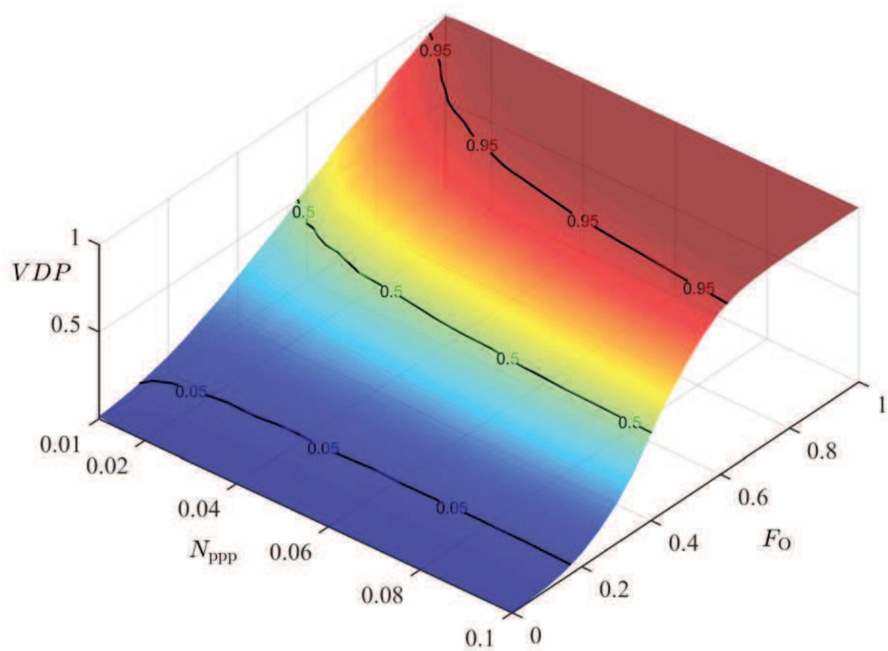

Fig. 6 Valid detection probability *VDP* as a function of the particle image density N_{ppp} and the loss-of-correlation due to out-of-plane motion F_{O} for an interrogation window size of $D_{\mathrm{I}} = 16$ pixel.

Figure 7 illustrates iso-contours with $VDP = 0.95$ for interrogation windows between 12^2 and 64^2 pixel. The solid lines in the figure show for each window size the acceptable value of F_O that results in $VDP = 0.95$ as a function of N_{ppp}. For smaller window sizes the VDP decreases and for larger ones the VDP increases. The dashed lines in Fig. 7 indicate the average number of particle images per interrogation window. The figure clearly shows that the condition $N_I F_O > 5$, as proposed by Keane and Adrian (1992), is not sufficient to achieve a high valid detection probability: For $N_I = 20$ and $N_{ppp} = 0.02$ the loss-of-correlation due to out-of-plane motion of $F_O \approx 0.5$ results in $VDP = 0.95$ although $N_I F_O \approx 10$, for example. The required effective number of particle images becomes even larger for cases with stronger out-of-plane motion and higher particle image density: For $N_I = 100$ and $N_{ppp} = 0.1$ the loss-of-correlation due to out-of-plane motion of $F_O \approx 0.4$ results in $VDP = 0.95$ although $N_I F_O \approx 40$. Furthermore, for $N_I F_O = 5$ (blue dotted line in Fig. 7) the loss-of-correlation due to out-of-plane motion must be $F_O > 0.8$ for the tested particle image density in order to achieve $VDP > 0.95$.

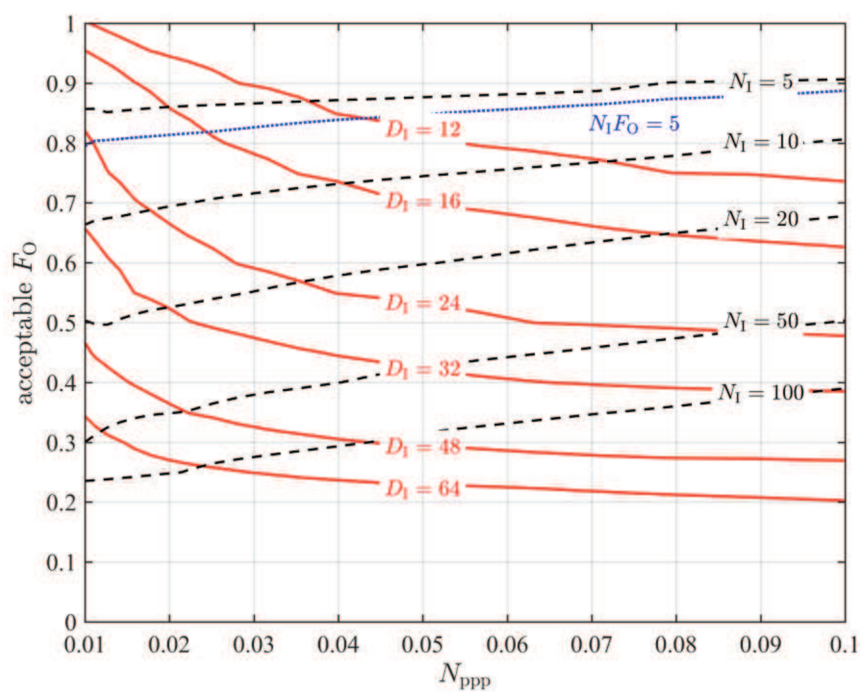

Fig. 7 Iso-lines with $VDP = 0.95$ showing the level of acceptable F_O with respect to the particle image density N_{ppp} for different interrogation window sizes (red solid lines). The dashed black lines indicate the required number of particle images within the interrogation window.

5. Summary & Conclusions

The analysis shows that the effective number of particle images $N_I F_I F_O$ is not sufficient to predict the valid detection probability of a PIV vector fields as proposed by Keane and Adrian (1992). This is because not only the number of particle images that can be paired must be considered but also the number of those that cannot be paired is important. The former determine the hight of the displacement peak and the latter contribute to the secondary correlation peak. Only if the number of paired particle images is large enough compared to the unpaired ones the correct correlation peak is the highest one.

From the variation of several parameters in Sec. 3 it can be concluded that the highest valid detection probability is reached if no motion is present at all and the particle image density is very low. However, this results in velocity measurements with high uncertainty and poor resolution. To achieve accurate measurement results some outlieres must be accepted (Scharnowski and Kähler, 2016a). An optimization regarding the spatial resolution and/ or the uncertainty must be performed during data acquisition (time separation between double images, optical magnification, aperture, light sheet width and energy, particle concentration, ...) as well as during data evaluation (interrogation window size, image deformation approach, vector post-processing, ...).

References

Adrian, R. J. (1997). Dynamic ranges of velocity and spatial resolution of particle image velocimetry. Measurement Science and Technology, 8(12), 1393.

Adrian, R. J., & Westerweel, J. (2011). Particle image velocimetry (No. 30). Cambridge University Press.

Cuvier, C., Srinath, S., Stanislas, M., Foucaut, J. M., Laval, J. P., Kähler, C. J., Hain, R., Scharnowski, S., Schröder, A., Geisler, R., Agocs, J., Röse, A., Willert, C., Klinner, J., Amili, O., Atkinson, C. & Soria, J. (2017). Extensive characterisation of a high Reynolds number decelerating boundary layer using advanced optical metrology. Journal of Turbulence, 18(10), 929-972.

Kähler, C. J., Scharnowski, S., & Cierpka, C. (2012). On the resolution limit of digital particle image velocimetry. Experiments in fluids, 52(6), 1629-1639.

Keane, R. D., & Adrian, R. J. (1990). Optimization of particle image velocimeters. I. Double pulsed systems. Measurement science and technology, 1(11), 1202.

Keane, R. D., & Adrian, R. J. (1992). Theory of cross-correlation analysis of PIV images. Applied scientific research, 49(3), 191-215.

Raffel, M., Willert, C. E., Scarano, F., Kähler, C. J., Wereley, S. T., & Kompenhans, J. (2018). Particle image velocimetry: a practical guide. Springer.

Scarano, F. (2001). Iterative image deformation methods in PIV. Measurement science and technology, 13(1), R1.

Scharnowski, S., & Kähler, C. J. (2016a). Estimation and optimization of loss-of-pair uncertainties based on PIV correlation functions. Experiments in Fluids, 57(2), 23.

Scharnowski, S., & Kähler, C. J. (2016). On the loss-of-correlation due to PIV image noise. Experiments in Fluids, 57(7), 119.

Sciacchitano, A., Scarano, F., & Wieneke, B. (2012). Multi-frame pyramid correlation for time-resolved PIV. Experiments in fluids, 53(4), 1087-1105.

Westerweel, J. (2008). On velocity gradients in PIV interrogation. Experiments in Fluids, 44(5), 831-842.